

# Summer diatom blooms in the eastern North Pacific gyre investigated with a long-endurance autonomous surface vehicle

Emily E. Anderson<sup>1</sup>, Cara Wilson<sup>2</sup>, Anthony H. Knap<sup>3</sup>  
and Tracy A. Villareal<sup>1</sup>

<sup>1</sup> Department of Marine Science and Marine Science Institute, The University of Texas at Austin, Port Aransas, TX, USA

<sup>2</sup> National Marine Fisheries, National Oceanic and Atmospheric Administration, Monterey, CA, USA

<sup>3</sup> Geochemical and Environmental Research Group, Texas A&M University, College Station, TX, USA

## ABSTRACT

Satellite chlorophyll *a* (chl *a*) observations have repeatedly noted summertime phytoplankton blooms in the North Pacific subtropical gyre (NPSG), a region of open ocean that is far removed from any land-derived or Ekman upwelling nutrient sources. These blooms are dominated by N<sub>2</sub>-fixing diatom-cyanobacteria associations of the diatom genera *Rhizosolenia* Brightwell and *Hemiaulus* Ehrenberg. Their nitrogen fixing endosymbiont, *Richelia intracellularis* J.A. Schmidt, is hypothesized to be critical to the development of blooms in this nitrogen limited region. However, due to the remote location and unpredictable duration of the summer blooms, prolonged in situ observations are rare outside of the Station ALOHA time-series off of Hawai'i. In summer, 2015, a proof-of-concept mission using the autonomous vehicle, *Honey Badger* (Wave Glider SV2; Liquid Robotics, a Boeing company, Sunnyvale, CA, USA), collected near-surface (<20 m) observations in the NPSG using hydrographic, meteorological, optical, and imaging sensors designed to focus on phytoplankton abundance, distribution, and physiology of this bloom-forming region. *Hemiaulus* and *Rhizosolenia* cell abundance was determined using digital holography for the entire June–November mission. *Honey Badger* was not able to reach the 30°N subtropical front region where most of the satellite chl *a* blooms have been observed, but near-real time navigational control allowed it to transect two blooms near 25°N. The two taxa did not co-occur in large numbers, rather the blooms were dominated by either *Hemiaulus* or *Rhizosolenia*. The August 2–4, 2015 bloom was comprised of 96% *Hemiaulus* and the second bloom, August 15–17, 2015, was dominated by *Rhizosolenia* (75%). The holograms also imaged undisturbed, fragile *Hemiaulus* aggregates throughout the sampled area at ~10 L<sup>-1</sup>. Aggregated *Hemiaulus* represented the entire observed population at times and had a widespread distribution independent of the summer export pulse, a dominant annual event suggested to be mediated by aggregate fluxes. Aggregate occurrence was not consistent with a density dependent formation mechanism and may represent a natural growth form in undisturbed conditions. The photosynthetic potential index (F<sub>v</sub>:F<sub>m</sub>) increased from ~0.4 to ~0.6 during both

Submitted 24 May 2018

Accepted 17 July 2018

Published 15 August 2018

Corresponding author

Tracy A. Villareal,  
tracyv@austin.utexas.edu

Academic editor

John Berges

Additional Information and  
Declarations can be found on  
page 21

DOI 10.7717/peerj.5387

© Copyright  
2018 Anderson et al.

Distributed under  
Creative Commons CC-BY 4.0

OPEN ACCESS

blooms indicating a robust, active phytoplankton community in the blooms. The diel pattern of  $F_v:F_m$  (nocturnal maximum; diurnal minimum) was consistent with macronutrient limitation throughout the mission with no evidence of Fe-limitation despite the presence of nitrogen fixing diatom-diazotroph assemblages. During the 5-month mission, *Honey Badger* covered ~5,690 km (3,070 nautical miles), acquired 9,336 holograms, and reliably transmitted data onshore in near real-time. Software issues developed with the active fluorescence sensor that terminated measurements in early September. Although images were still useful at the end of the mission, fouling of the LISST-Holo optics was considerable, and appeared to be the most significant issue facing deployments of this duration.

**Subjects** Ecosystem Science, Marine Biology, Biological Oceanography

**Keywords** Remote sensing, Diatom bloom, Oligotrophic ocean, Marine, Symbiosis, Phytoplankton, Autonomous vehicle, Diatoms

## INTRODUCTION

Low-nutrient, low chlorophyll oceanic regimes with chlorophyll *a* (chl *a*) concentrations <0.07 mg m<sup>-3</sup> constitute approximately 60% of the world ocean ([Guieu et al., 2014](#)) and are home to a phytoplankton community highly adapted for survival at the ambient nanomolar concentrations of inorganic NO<sub>3</sub><sup>-</sup> and PO<sub>4</sub><sup>3-</sup>. One of the important adaptations is nitrogen-fixation (diazotrophy), a process by which dissolved N<sub>2</sub> is converted into ammonium for incorporation into amino acids and proteins ([Carpenter & Capone, 2008](#)). Diazotrophy requires abundant iron resources ([Mills et al., 2004](#); [Ratten et al., 2015](#)) and is reduced in iron-limited regions. N<sub>2</sub>-fixation may also be limited by other nutrients ([Kustka, Carpenter & Sanudo-Wilhelmy, 2002](#); [Mills et al., 2004](#); [Ratten et al., 2015](#)) or competition by non-diazotrophic phytoplankton ([Weber & Deutsch, 2014](#)). Multiple prokaryote taxa are capable of diazotrophy ([Zehr & Kudela, 2011](#)); photosynthetic taxa include colonial cyanobacteria such as *Trichodesmium* spp. ([Capone et al., 1997](#); [Goering, Dugdale & Menzel, 1966](#)), free-living coccoid forms including *Crocospheara watsonii* ([Goebel et al., 2008](#); [Zehr et al., 2001](#)), and coccoid or filamentous forms symbiotic with eukaryotes. Of these latter symbioses, there are coccoid forms symbiotic with the prymnesiophyte *Braarudosphaera bigelowii* (Gran and Braarud) Deflandre ([Thompson et al., 2012, 2014](#)), dinoflagellates ([Farnelid et al., 2010](#); [Foster, Carpenter & Bergman, 2006](#)) and filamentous or coccoid cyanobacteria occurring as exo- or endosymbionts of diatoms ([Foster & O'Mullan, 2008](#); [Villareal, 1992](#)). This latter group, diatom-diazotroph associations (DDAs), are dominated by an endosymbiosis between the filamentous cyanobacteria, *Richelia intracellularis*, and members of the diatom genera *Rhizosolenia* and *Hemiaulus*. These symbioses have complex interactions with their hosts ([Foster & Zehr, 2006](#); [Hilton et al., 2013](#)) and the taxonomic distinctness of the symbionts even within a single host genus remains unclear. DDAs play important roles in biogeochemical cycling off the Amazon ([Carpenter et al., 1999](#); [Subramaniam et al., 2008](#)) and Mekong Rivers ([Bombar et al., 2011](#)) as well as in the central North Pacific gyre ([Church et al., 2008](#)).

At the Hawai'i Ocean Time-series (HOT), episodic pulses of DDAs dominated by *Hemiaulus* spp. rapidly sink to depth (Scharek *et al.*, 1999; Scharek, Tupas & Karl, 1999) and transport ~20% of the annual benthic carbon flux in a limited window (July 15–August 15) termed the summer export pulse (Karl *et al.*, 2012). Isotopic signatures of N<sub>2</sub> fixation suggest that their diazotrophic symbiont is present and fueling the biomass flux; the rapid sinking rate indicates aggregation plays a key role in the accelerated transport to depth (Scharek, Tupas & Karl, 1999). The summer export pulse is possibly linked to episodic surface blooms of DDAs advecting through the region in the prevailing flow (Dore *et al.*, 2008; Fong *et al.*, 2008; White, Spitz & Letelier, 2007). Auxospore formation has also been offered as an explanation (Karl *et al.*, 2012) although direct examination of trap material (Scharek *et al.*, 1999; Scharek, Tupas & Karl, 1999) reported no evidence of auxosporulation. Follett *et al.* (2018) modeled generalized diatom-diazotroph association dynamics, noting that the population peaked in the early summer and rapidly declined during the summer export pulse window after a transition from modelled Fe to P limitation favored competitive exclusion by other taxa. The model necessarily addressed generalized conditions and did not address the localized blooms noted by satellites. These blooms dominate in the summer (Wilson, 2003) and are often associated with the unique properties of mesoscale eddy flow-fields (Calil *et al.*, 2011; Calil & Richards, 2010; Guidi *et al.*, 2012). There are few long-term, high frequency direct observations on diatom-diazotroph association abundance to evaluate these hypotheses.

In the North Pacific, the diatom-diazotroph association host genus *Hemiaulus* is a characteristic upper euphotic zone species typically found across the central North Pacific gyre at concentrations of  $\sim 10^2$  cells L<sup>-1</sup> (Venrick, 1988, 1999). Near-surface blooms of both *Rhizosolenia* and *Hemiaulus* DDAs at 10<sup>4</sup> cells L<sup>-1</sup> (Venrick, 1974) extend well north of Hawai'i at abundance up to 10<sup>4</sup> L<sup>-1</sup> (Brzezinski, Villareal & Lipschultz, 1998; Krause *et al.*, 2012; Villareal *et al.*, 2011) and are frequently associated with summer chl *a* blooms observed in satellite ocean color sensors (Villareal *et al.*, 2011). These chl *a* blooms (operationally defined as  $> 0.15$  mg chl *a* m<sup>-3</sup>) north of 25.5°N cover a much greater range of temperatures and surface area than the blooms at HOT ( $\sim 22.5$ °N) and extend at least as far north as 35.5°N (Villareal *et al.*, 2012). While the data suggest that these satellite-observed blooms are probably associated with diatom-diazotroph association events, it has remained difficult to sample these more northerly blooms due to the remote location, episodic timing and extensive geographic range. The applicability of the summer export pulse to these areas is unclear, as is the general role of aggregation in *Hemiaulus* spp. biology. In situ diver observations suggest aggregation commonly occurs in *Hemiaulus* (Villareal *et al.*, 2011), providing a means for rapid sinking as the bloom senesces. It is unclear whether *Hemiaulus* aggregation occurs as a density dependent process as noted in coastal diatom blooms (Burd & Jackson, 2009; Jackson, 2005), is a natural growth form of the genus similar to *Rhizosolenia* mats, is uniquely localized to the summer export window, or is a more generalized feature throughout the year. With recent observations of the ubiquitous presence of living diatom cells in the 2,000–4,000 m depth strata, the role of aggregation in oceanic diatom biology has assumed new importance (Agusti *et al.*, 2015).

Sampling these blooms outside of HOT is a challenge due to both the distance to blooms, unpredictable occurrence, long planning lead time, and cost involved in multiple week research cruises. Even at HOT, shipboard sampling is at approximately monthly intervals and insufficient to resolve episodic events in annual cycles. To address this, we used an SV2 Wave Glider (*Honey Badger*), a long-range autonomous vehicle utilizing wave power for propulsion and solar panel arrays on a surface float to provide power for a variety of sampling instruments (Daniel, Manley & Trenaman, 2011). While many types of autonomous vehicles are used in the marine environment (Dickey et al., 2008; Lee et al., 2017), the Wave Glider is particularly capable of multiple-month missions carrying extensive payloads, is under near-real time control, and has successfully transited from Hawai'i to Australia while returning oceanographic data (Villareal & Wilson, 2014). They have been successfully deployed for sediment transport studies (Van Lancker & Baeye, 2015), wind/current assessments of typhoons (Van Lancker & Baeye, 2015), buoy validation exercises (Fitzpatrick et al., 2015), examination of air-sea coupling in the Southern Ocean (Thomson & Girton, 2017), and processes controlling North Atlantic and Eastern Pacific Ocean salinity variability (Lindstrom et al., 2017).

In our study, we equipped the Wave Glider *Honey Badger* with a novel array of imaging and photophysiology sensors specifically targeting phytoplankton dynamics. We present data gathered during a 5-month mission in 2015 which sampled two diatom blooms. The mission objectives were to return the glider after 5 months with all sensors collecting useful data, determine if a holographic imaging system could quantify diatom events, relate the abundance to satellite observed chl *a* blooms, examine the data for *Hemiaulus* aggregations, and acquire photosynthetic efficiency data using active fluorescence.

## MATERIALS AND METHODS

The mission area for the *Honey Badger* was the eastern North Pacific subtropical gyre (NPSG) spanning 19–30°N and 144–157°W in the open waters northeast of the Hawaiian Islands (Fig. 1) where chl *a* blooms regularly occur between July and October (Wilson, 2003). Waypoints were chosen based on Aqua-MODIS 8-day composite chl *a* concentration satellite images from the Environmental Research Division's ERDDAP (<https://coastwatch.pfeg.noaa.gov/erddap/griddap/erdMBchl8day.html>). After a preliminary deployment in the test area off Kawaihae, Hawai'i, the *Honey Badger* headed north on June 1, 2015. It was recovered on November 3, 2015 and returned to the test facility for evaluation and data download.

The Wave Glider® SV2 (Liquid Robotics, a Boeing company, Sunnyvale, CA, USA) is an autonomous surface vehicle capable of extended operations offshore. It has a surface float (2.1 × 0.6 m) connected by an umbilical (seven m in this application) to a subsurface glider (0.4 × 1.9 m) with articulating wings (1.1 m wide) that uses vertical motion from waves to provide forward movement. Within the surface float, equipment bays provide space for computers, communications equipment and battery arrays powered by solar panels. Iridium satellite communication with the Wave Glider *Honey Badger* used in this mission was in near-real time and provided a near immediate ability to course correct and respond to environmental conditions.

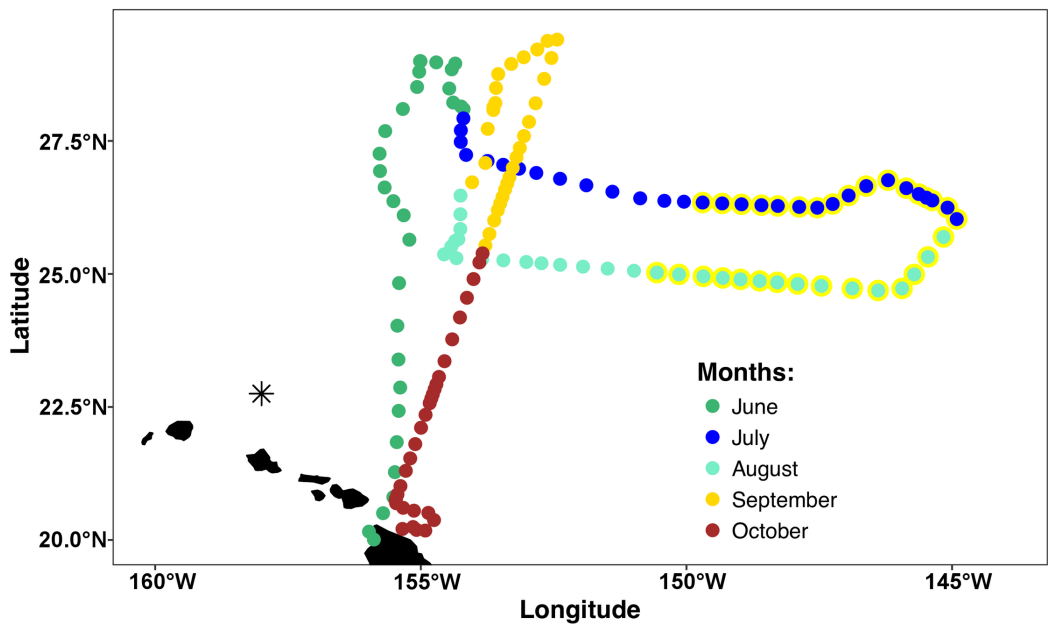


**Figure 1** Mission track of the SV2 Wave Glider *Honey Badger*. Mid-day positions points are color-coded by month. The asterisk north of Oahu is Station ALOHA of the Hawai'i Ocean Time-Series (HOT).

Full-size DOI: [10.7717/peerj.5387/fig-1](https://doi.org/10.7717/peerj.5387/fig-1)

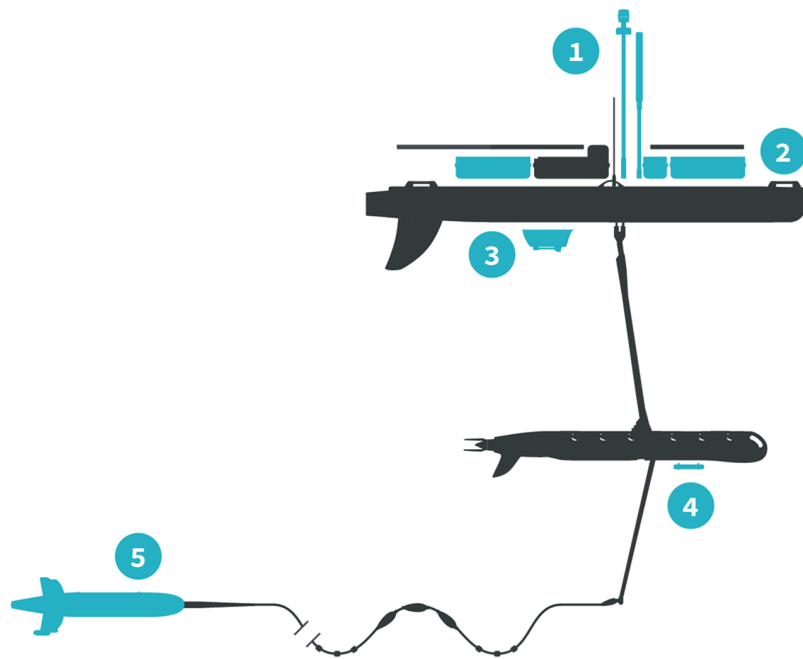


**Figure 2** *Honey Badger* diagram and sensor locations. Schematic provided courtesy of Liquid Robotics, a Boeing Company.

Full-size DOI: [10.7717/peerj.5387/fig-2](https://doi.org/10.7717/peerj.5387/fig-2)

The *Honey Badger* was equipped with sensors on the float, the sub-body, and on a towed body (Fig. 2; Table 1). The float contained two Turner Designs C3 fluorometers (Turner Designs, Sunnyvale, CA, USA) rimmed with anti-fouling copper, a Seabird Electronics

**Table 1** List of the instruments onboard the *Honey Badger* with their locations on the Wave Glider (Fig. 2) and their programmed sample frequency.

Sensor (location)	Variables (units)	Interval	Available in near real time?
Sea-bird scientific's gpCTD (2)	Water temperature (°C), salinity, density (dBar)	48 h <sup>-1</sup>	Yes
Turner Designs' C3 <sup>TM</sup> submersible fluorometer with antifouling coating (2)	Colored dissolved organic mater (CDOM) (RFU), chlorophyll-a (RFU), and phycoerythrin fluorescence (RFU)	6 h <sup>-1</sup>	Yes
Turner Designs' C3 <sup>TM</sup> submersible fluorometer without antifouling coating (2)	Colored dissolved organic mater (CDOM) (RFU), chlorophyll-a (RFU), and phycoerythrin fluorescence (RFU)	6 h <sup>-1</sup>	Yes
AirMar Technology's WX series ultrasonic WeatherStation <sup>®</sup> (1)	Air temperature (°C), pressure (mBar), average wind speed (knots) and direction (degrees true)	6 h <sup>-1</sup>	Yes
Datawell BV's MOSE (2)	Significant wave height (m) and direction (degrees true)	2 h <sup>-1</sup>	Yes
Cannon G10 camera (2)	Downward facing camera for imaging the sub-body	6 h <sup>-1</sup>	No
Turner Designs' PhytoFlash (4)	F <sub>o</sub> , F <sub>m</sub> , F <sub>v</sub> , yield (F <sub>v</sub> :F <sub>m</sub> )	6 h <sup>-1</sup>	Yes
Sequoia Scientific LISST-Holo (5)	Holographic microscopic images of the water	1 Burst of 15 images every 6 h	No

gpCTD (Seabird Electronics, Inc., Bellevue, WA, USA) for water temperature and salinity with an inline antifouling tablet, a Canon G10 camera (Canon, USA Inc., Melville, NY, USA) looking down through the float, a Datawell MOSE weather sensor (Datawell BV, Haarlem, The Netherlands), Airmar WX and WS weather sensors+light bar (Airmar Technology Corporation, Milford, NH, USA), an automatic identification system (AIS) transponder, and a radar reflector. The sub-body located seven m below the float had an externally mounted Turner Designs PhytoFlash (Turner Designs, Sunnyvale, CA, USA) utilizing the data and power connections through the umbilical. The PhytoFlash sensor was shielded by a dark cap painted inside and out with anti-fouling paint. A Sequoia Scientific, Inc. (Bellevue, WA, USA) Laser in situ Scattering and Transmissometry Holographic System (LISST-Holo, termed Holo) was deployed in a neutrally buoyant towed body behind the *Honey Badger* on a 10 m tether equipped with scoops to passively direct water into the sample field. The tow fish varied from 6.3 to 15.5 m deep based on the Holo's internal depth sensor. The Holo drew power from the umbilical with the data stored in the Holo's onboard internal memory module. Bandwidth limitations did not permit transmission to shore via Iridium satellite. The Holo sample chamber was painted with antifouling paint and lined with copper tape on other surfaces to minimize fouling. Power consumption and available solar charging dictated sampling frequency and varied with the sensors (Table 1). The vehicle reported location and condition telemetry every 30 s. Sensors were integrated into the onboard processing and communications equipment by

Liquid Robotics with the exception of the PhytoFlash. Software integration for the PhytoFlash and tow body construction was provided by the Geophysical Engineering Research Group (GERG) at Texas A&M University.

The Turner C3 fluorometers were equipped with excitation and emission filters for chl *a*, phycoerythrin, and colored dissolved organic material (CDOM) with values reported in fluorescence units. The C3 sensors were deployed on either side of the centerline with a port and starboard sensor. The port C3 sensor and optical port for the look-down camera were coated with a ~30  $\mu\text{m}$  layer of ClearSignal antifouling compound (Severn Marine Technologies, Annapolis, MD, USA) in spring, 2014. Due to technical difficulties, the mission was delayed a year with unknown effects on the viability of the coating. The look-down camera began recording on July 1, 2015 and imaged vertically below the float for examining the umbilical and glider as needed but also captured images of fish and biofouling over the course of the mission.

The Holo uses collimated laser light to create refraction patterns from particles that are then recorded by camera to create a hologram (Davies *et al.*, 2015). Software provided by Sequoia Scientific Inc. (Holo\_Batch v. 3.1) reconstructed multiple holograms into grayscale images. Particle biovolume was calculated based on a cross-section area projected into a sphere. Holo\_Detail (v. 3.1) was used to process each hologram in greater detail to identify *Hemiaulus* and *Rhizosolenia* spp. Isolated hologram areas could be imaged individually as 0.1–1 mm thick sections allowing detailed images layer by layer. The sampling rate of 15 holographic images (30 s between images) every 6 h was set prior to launch based on worst case power consumption calculations and could not be modified once underway. The 15-image bursts taken every 6 h were combined to form one record yielding four records (bursts)  $\text{d}^{-1}$ . The Holo sampling volume was 1.86 mL per image with the 15-image burst sampling a total of 27.9 mL. Dye studies prior to the mission indicated the 30 s between images was sufficient for full chamber volume replacement.

The large file size (~2 MB) of each raw Holo hologram precluded satellite transmission and were only available for analysis after the *Honey Badger*'s recovery in November 2015. Upon recovery of the drive, 9,336 holographic images were analyzed with the Holo\_Batch and Holo\_Detail at the University of Texas at Austin's Marine Science Institute. Comparison of Holo\_Batch processing and individual Holo\_Detail processing of the same images indicated progressive loss of recognizable diatoms over the mission due to biofouling (examples given in Fig. S1). Therefore, *Hemiaulus* and *Rhizosolenia* cells were quantified using the Holo\_Detail software on every hologram with distinctive diffraction patterns indicating when particles were present. While using the Holo\_Detail to enumerate diatoms was more time-intensive than using the montages of in-focus particles produced by the Holo\_Batch, it was necessary as the montages often failed to show *Hemiaulus* or *Rhizosolenia* cells when they were clearly identifiable in Holo\_Detail. The small size of individual *Hemiaulus* cells (~15  $\mu\text{m}$ ) and light silicification also contributed to difficulties in using the batch analysis mode as biofouling interference increased.

The Holo's sampling capability allowed counting cells with a minimum concentration of 36 cells  $\text{L}^{-1}$ . Individual *Hemiaulus* cells were at the size threshold of the Holo and hard to differentiate from other small cells unless they were in recognizable chains.

In addition, *Hemiaulus* cells occurred as both individual chains and aggregations of various size. Chains were defined as three or more *Hemiaulus* cells which formed a curve with clear ends which did not cross itself or others more than once. Aggregates were defined as *Hemiaulus* cells in a chain or multiple chains with multiple ends or no discernable ends which crossed itself, other chains, or other particles multiple times.

Hologram processing also returned calculated biovolume for all detected particles after calculating their equivalent spherical diameter. The biovolume was automatically separated into bins based on equivalent spherical diameter from 2.5 to 9,847  $\mu\text{m}$  (50 bins with the upper size limit of each bin being 1.18 times the lower limit). The diatoms of interest in this study have an equivalent spherical diameter between 13 and 60  $\mu\text{m}$  so a subset of bins (13.1–58.1  $\mu\text{m}$ ) were chosen to focus the analysis. Holograms with schlieren (optical anomalies in transparent mediums), microbubbles or blank images were manually removed from the analyses.

Biofouling interference was removed using the manufacturer's recommended procedure to average the biovolume over large groups of images. This procedure generated a constant signal that represented a consistent particle presence assumed to be biofouling. We arbitrarily averaged groups of 510 holograms representing an 8.5-day window for a total of 14 background signatures. This signature was subtracted from each hologram in the specified window to generate a biofouling-corrected biovolume. Details of this correction and effects on the result are included as [Supplemental Information](#) and [Figs. S1](#) and [S2](#).

Pulse amplitude modulation fluorometry ([Schreiber, 2004](#)) determination of  $F_v:F_m$  (PhytoFlash sample frequency = 6 samples  $\text{h}^{-1}$ ) was used to evaluate phytoplankton photophysiology. The PhytoFlash sampled at 10 min intervals but was accelerated to 1 min intervals from July 27 to 28 to test the system's resiliency to increased sampling rates. The port C3 sensor was on a fixed 10 min sampling interval with 10 samples averaged to generate a single value. The starboard sensor was reprogrammable via remote communications and was varied in sampling timing and averaging at various points in the mission. Changes from multi-point averaging to single point reporting resulted in systematic and predictable baseline shifts. The reasons for these changes are unknown. Iron stress was evaluated using the variable fluorescence criteria of [Behrenfeld & Milligan \(2013\)](#) simplified for the lower sampling rate of the PhytoFlash. In a macronutrient limited environment with sufficient iron, the nocturnal  $F_v:F_m$  is greater than the diurnal  $F_v:F_m$ . In an iron limited environment, the reverse is true. Time averaging (night time average of 36 data points; 08:00–13:59 UTC and daytime average of 54 data points; 18:00–02:59 UTC) was required to obtain a stable signal and timed to avoid the observed crepuscular  $F_v:F_m$  excursions. The PhytoFlash shutdown and missed samples at an increasing frequency during the mission and eventually failed completely in early September (traced to software issues). To ensure a comparable day/night sampling, only periods with 75% or more of the expected number of samples were included in the iron-limitation analysis and both periods for a date were required to meet the above standard. These criteria resulted in the removal of 33 of the 94 days of data collected over the mission. The entire  $F_v:F_m$  dataset was plotted vs time for a visual inspection of the data as well.

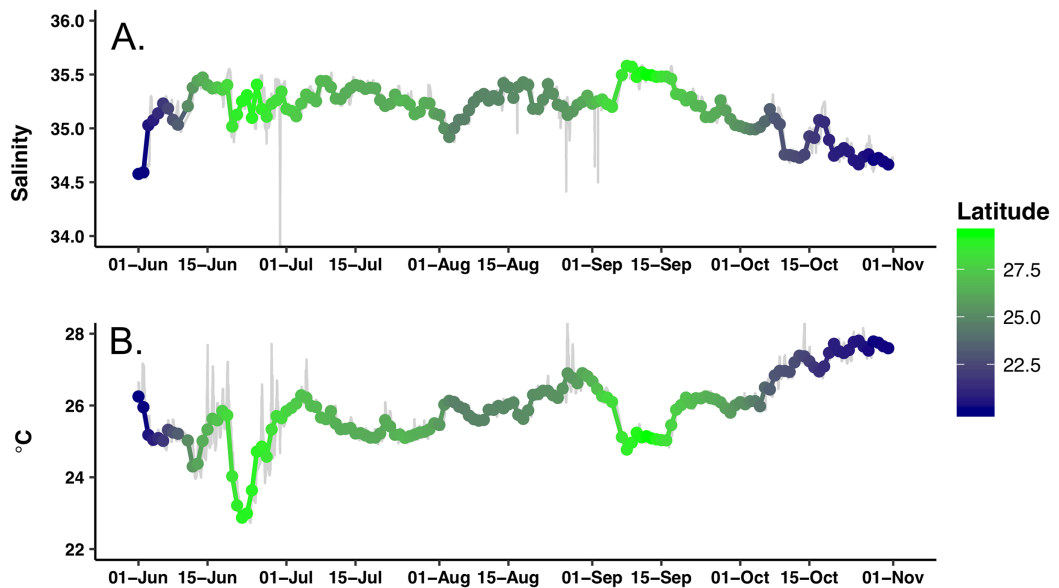


**Figure 3** Time series of the hydrographic properties from the *Honey Badger*'s gpCTD sensor. (A) Salinity. (B) Temperature (°C). The gray lines are the data with a nine-point smoothing, the color-coded dots are daily average values.

[Full-size](#) DOI: 10.7717/peerj.5387/fig-3

Aqua MODIS satellite's 8-day composite of daily chl *a* was used to produce an animation showing the development of the blooms in the NPSG during the 2015 bloom season (June–November) and the position of the *Honey Badger*'s track (Video S1 at [https://figshare.com/articles/S1\\_movie\\_mp4/5993644](https://figshare.com/articles/S1_movie_mp4/5993644)). The raw data from the C3s, gpCTD, AIS, MOSE, PhytoFlash, and weather station are archived at BCO-DMO (<http://www.bco-dmo.org/project/505589>). The BCO-DMO site also contains the raw holograms, the biovolume data, as well as the *Hemiallus* and *Rhizosolenia* abundance data.

## RESULTS

Extensive biofouling on several of the optical windows occurred during the mission. A time series of images from the look down camera illustrates the development over time of barnacles and associated organisms (Fig. S3). A metal incompatibility with internal screw in the LISST-Holo camera system mount resulted in significant corrosion (Fig. S4); however, it did not encroach into the sample plane and no data was lost. *Honey Badger* collected 5 months of salinity, surface water temperature, diatom abundance, photophysiology, and biovolume data from the NPSG. A nine-point running average (Fig. 3, gray line) and daily average were used to remove changes due to rain events or sensor errors in the gpCTD. The daily averaged water salinity and temperature data (Fig. 3, color-coded by latitude) ranged from 22.8 to 27.8 °C, and 34.6–35.6 salinity. The lower salinity water near Hawai'i is evident at the beginning and ending of the mission. The *Honey Badger* did not cross the sub-tropical front, which is characterized by salinity ~34.5 found at ~30°N (Wilson et al., 2013). The pronounced temperature-salinity gradient from the center of the gyre to Hawai'i is evident in the continuous decrease in salinity and increase in temperature along the straight line transect from the farthest north point

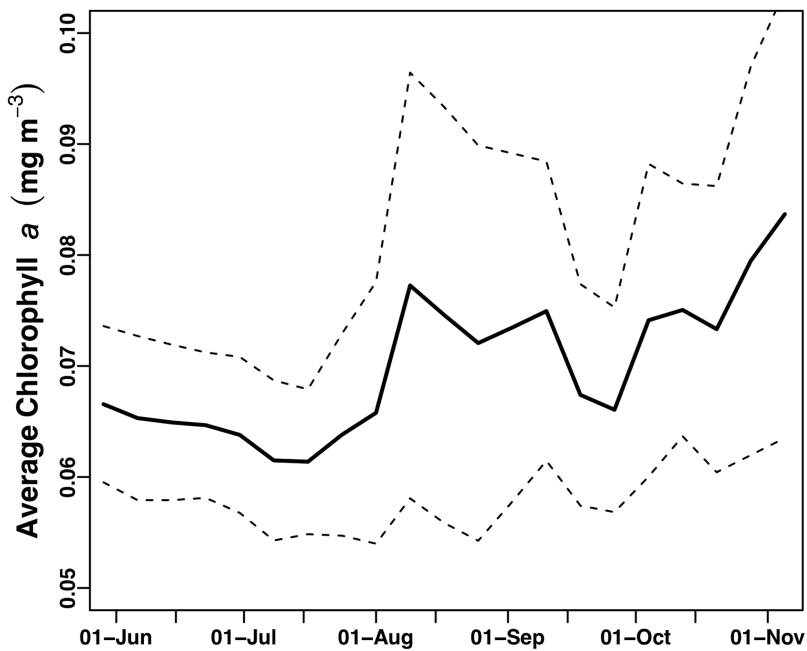


**Figure 4** Average chl *a* concentration of the study area over time. All chl *a* per pixel values from Aqua MODIS 8-day composite data within the study area (bounded by 19 to 30°N and 157–144°W) were averaged to generate a single daily value for the study area. Solid line = average chl concentration for the study area. Dashed lines = average chl concentration  $\pm$  1 s.d.

[Full-size](#) DOI: [10.7717/peerj.5387/fig-4](https://doi.org/10.7717/peerj.5387/fig-4)

(29.245°N and 152.40°W) on September 12, 2015 to just north of Hawai'i on October 23, 2015 (20.67°N and 155.47°W).

The study area underwent a general chl *a* increase over the course of the mission that was evident visually as a shift from deep blue to light green in mid-July (Video S1). This increase was quantitatively expressed as the average of chl *a* values from all pixels in the study area (Fig. 4). Following a period of uniformly low chl *a* concentration throughout the study area in June–July 2015 (Fig. 4), in mid-July chl *a* concentrations throughout the study area increased concurrent with increased chl *a* variability (increased standard deviation around the mean) due to chl *a* blooms (Video S1). This period of elevated bloom activity extended from August 1 to September 15. During this period, there were multiple blooms evident where the satellite chl *a* exceeded 0.2 mg m<sup>-3</sup>. The brief decrease in late September was followed by an increase in average chl *a* through the end of the mission.

The two float-mounted Turner C3 fluorometers produced erratic signals and random shifts in baseline values (Fig. 5). The sensors did not parallel each other except for a general increase in the cyanobacteria pigment phycoerythrin from September 21, 2015 to the end of the mission, nor did the satellite chl *a* values at *Honey Badgers* location note similar fluctuations. The C3 data sets were excluded from further analysis due to a lack of an independent diagnostic test to determine which data points were reflective of the water properties and which were noise or errors introduced by the sensor.

*Hemiaulus* and *Rhizosolenia* cells were readily identifiable in the processed holograms both as chains and aggregates (Fig. 6). *Hemiaulus* cells were identifiable as either curved or

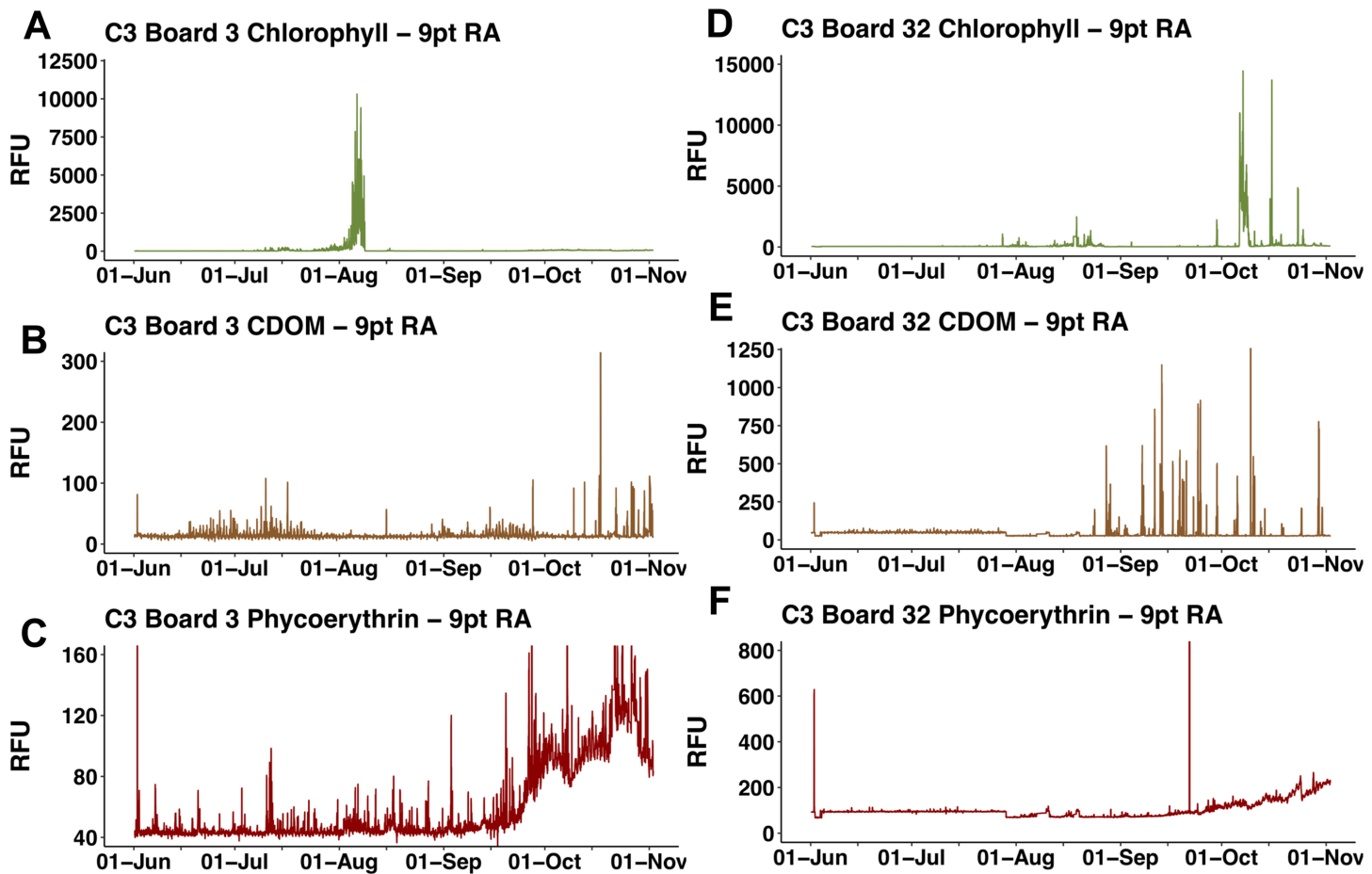


**Figure 5** C3 fluorometer data from the *Honey Badger*. Note scale shifts between plots. (A–C) Sensor coated with antifouling compound. (A) Chl. (B) CDOM. (C) Phycoerythrin. (D–F) Uncoated sensor. (D) Chl. (E) CDOM. (F) Phycoerythrin. Study site: RFU, relative fluorescence units.

Full-size DOI: 10.7717/peerj.5387/fig-5

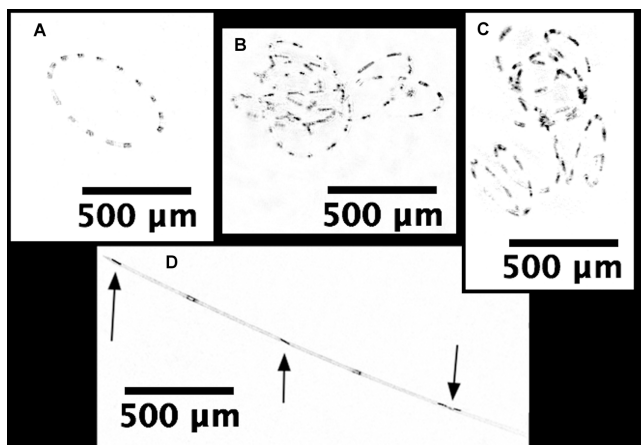


**Figure 6** Processed holographic images of *Hemiaulus* and *Rhizosolenia* cells and aggregates. (A) Curved chain of *Hemiaulus hauckii*. Each dark dot is the cell mass separated from adjacent cells by siliceous structures. Images have been contrast enhanced for clarity. (B) *Hemiaulus* aggregate. (C) *Hemiaulus* aggregate. (D) Two complete *Rhizosolenia* cells and half of the next cell with their symbionts *Richelia* (arrows) located at the apex of the cells.

Full-size DOI: 10.7717/peerj.5387/fig-6

spiral chains (Fig. 6A) as well as aggregates of varying degrees of complexity (Figs. 6B and 6C). With three cells required to define identify a *Hemiaulus*, the minimum reported concentration is 108 cells L<sup>-1</sup>. In *Rhizosolenia*, the symbiont of *Richelia intracellularis* was visible as well (Fig. 6D arrows). Mean *Hemiaulus* abundance over the entire mission was 303 cells L<sup>-1</sup> (s.d. =  $1.0 \times 10^3$  cells L<sup>-1</sup>, n = 610) and mean *Rhizosolenia* abundance was 63 cells L<sup>-1</sup> (s.d. =  $2.7 \times 10^2$  cells L<sup>-1</sup>, n = 610) over all the samples. However, of the 610 samples, only 208 contained *Hemiaulus* cells and 207 contained *Rhizosolenia* cells. When present, the average *Hemiaulus* abundance was  $8.9 \times 10^2$  L<sup>-1</sup> (s.d. =  $1.6 \times 10^3$  cells L<sup>-1</sup>, n = 208). Of the samples containing *Rhizosolenia* cells, the average abundance was  $1.8 \times 10^2$  cells L<sup>-1</sup> (s.d. =  $4.5 \times 10^2$  cells L<sup>-1</sup>, n = 207). *Hemiaulus* maximum abundance in the averaged 15 image burst was  $1.4 \times 10^4$  cells L<sup>-1</sup> on August 2, 2015 and the *Rhizosolenia* maximum abundance was  $2.8 \times 10^3$  cells L<sup>-1</sup> on August 16, 2015 (Fig. 7). Blooms were defined operationally as occurring when the abundance value was two s.d. above the mean present values, resulting in a threshold of  $4 \times 10^3$  cells L<sup>-1</sup> for *Hemiaulus* and  $1 \times 10^3$  cells L<sup>-1</sup> for *Rhizosolenia*.

Surface chl *a* (satellite derived) at *Honey Badger*'s position underwent a ~2-fold variation over the mission (Fig. 7A) with a sharp increase on August 2, 2015, followed by considerable day to day patchiness evident throughout the rest of the mission. A similar pattern was seen in the Phytoflash F<sub>m</sub> data from sub body at ~7 m (Fig. 7B) until the data collection failed on September 1, 2015. Two blooms were sampled, a *Hemiaulus* bloom on August 2–4, 2015 and a *Rhizosolenia* bloom on August 15–17, 2015. Diatom abundance (Figs. 7C and 7D) was patchy with two order of magnitude changes occurring within between adjacent Holo bursts in the blooms, a distance of approximately 10 km. The *Hemiaulus* bloom was dominated by *Hemiaulus* (96% of total diatoms; Fig. 7C) while the *Rhizosolenia* bloom was dominated by *Rhizosolenia* (75% of total diatoms; Fig. 7D). However, neither bloom reached the 0.15 mg m<sup>-3</sup> chl *a* threshold used to identify a satellite chl *a* bloom. The two blooms were separated in space and in time (Figs. 7 and 8) and both had increases in biovolume (Fig. 7E). The larger *Rhizosolenia* cells contributed nearly 2/3 more biovolume on August 15–17, 2015 despite the cell numbers being only 1/3 that of the *Hemiaulus* bloom. The satellite chl *a* signature was still faint when *Honey Badger* sampled the *Hemiaulus* bloom from August 2 to 4, 2015 (compare Figs. 8A and 8B) but continued to develop after the *Honey Badger* left the area (Video S1). The *Rhizosolenia* bloom sampled by the *Honey Badger* from August 15 to 17, 2015 did not have a well-defined satellite chl *a* signal (Figs. 7A, 7C and 8B). However, the PhytoFlash F<sub>m</sub> (Fig. 7F) was approximately 33% higher in the *Rhizosolenia* bloom than the *Hemiaulus* bloom.

Two declining blooms evident in the chl *a* animation were sampled (August 23–25, 2015 and September 14–16, 2015; Video S1). In both cases, no aggregates were seen in the Holo and the maximum local abundance ~300 cells L<sup>-1</sup> was reached in only one burst in each area. The rest of the bursts were devoid of *Hemiaulus*. However, the lookdown camera imaged what appeared to be a mass occurrence of small white flocs (Fig. S3B). Their identity could not be confirmed, but the size and shape are consistent with either marine aggregates or possibly colonial radiolarians.

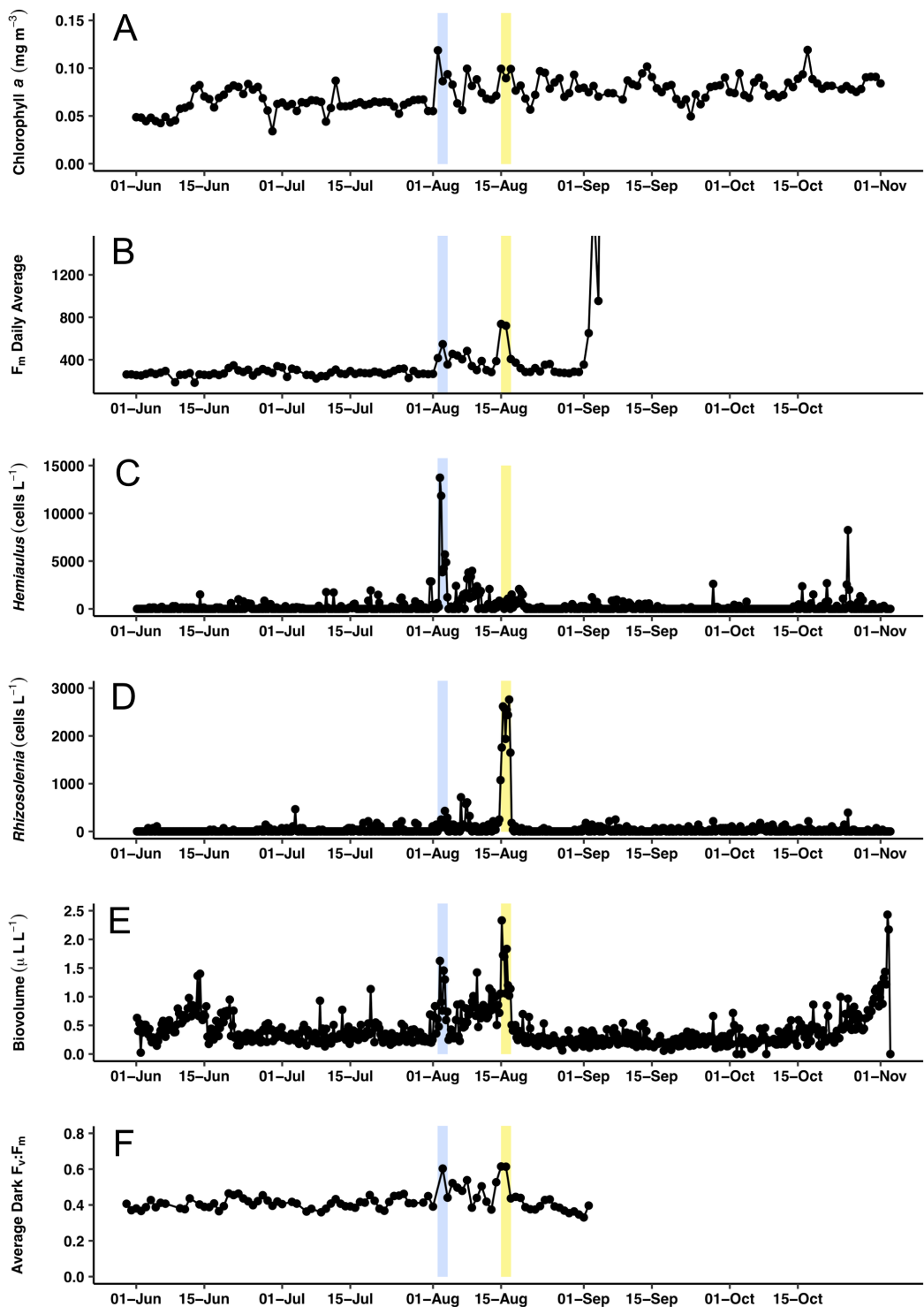


**Figure 7** Time series comparisons between the Aqua MODIS *a* and the in situ data collected by the *Honey Badger's* sensors. (A) 8-day composite data from Aqua MODIS showing surface chl *a* concentrations ( $\text{mg m}^{-3}$ ) near *Honey Badger's* location. (B) Average daily  $F_m$  (maximum fluorescence) from the Phytoflash. (C) *Hemiaulus* abundance ( $\text{cells L}^{-1}$ ). (D) *Rhizosolenia* abundance ( $\text{cells L}^{-1}$ ). (E) Biovolume from 11–58  $\mu\text{m}$  bins. (F) Average  $F_v:F_m$  between 08:00–13:59 UTC (dark-adapted value). Blue and yellow shaded area indicate the *Hemiaulus* and *Rhizosolenia* bloom, respectively.

Full-size DOI: 10.7717/peerj.5387/fig-7

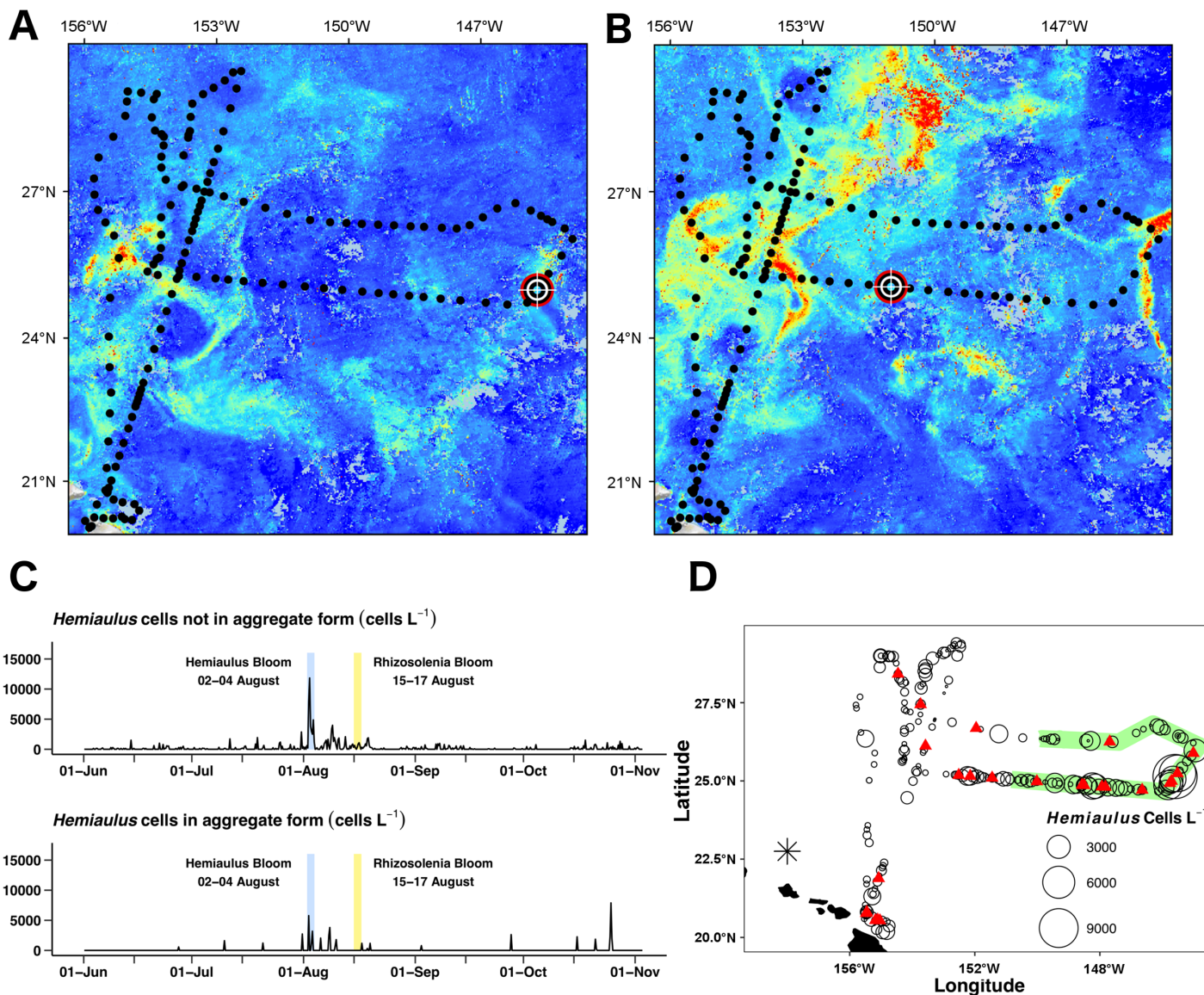


**Figure 8** *Hemiaulus* aggregated and free-living form distribution. (A) and (B) Aqua MODIS chlorophyll surface concentration and *Honey Badger*'s position. Black dot = mission track position, red-white-black crosshair = *Honey Badger*'s position on day of satellite image. (A) August 3, 2015; *Hemiaulus* bloom. (B) August 16, 2015; *Rhizosolenia* bloom. (C) Time-series plot of *Hemiaulus* abundance in the free-living or aggregated form. (D) Locations of non-aggregated *Hemiaulus* cells and locations of aggregates. Red triangle = aggregate. Circles = non-aggregated *Hemiaulus* cells L<sup>-1</sup>, size is proportional to abundance. The green area indicates where *Honey Badger* sampled during the SEP time window (15 July–15 August).

Full-size DOI: 10.7717/peerj.5387/fig-8

Maximum F<sub>v</sub>:F<sub>m</sub> values (~0.6) were associated with the *Hemiaulus* and the *Rhizosolenia* peak abundance values (Fig. 7E) although the data loss on August 2 may have missed higher F<sub>v</sub>:F<sub>m</sub> values. During the period of the two blooms (August 2–17), the F<sub>v</sub>:F<sub>m</sub> values underwent day to day changes in magnitude that were visibly distinct from the period before and after.

The Holo captured 31 *Hemiaulus* aggregates in 23 sampling bursts (Table 2; Figs. 8C and 8D) out of 610 total bursts over the mission (3.8%) or 11% of samples when any

**Table 2** *Hemiaulus* aggregate locations and contribution to total *Hemiaulus* abundance.

Aggregate events outside the SEP				Aggregate events within the SEP					
Date (UTC)	n	Location		% <i>Hemiaulus</i> in Aggregates (total cells L <sup>-1</sup> )	Date (UTC)	n	Location		% <i>Hemiaulus</i> in aggregates (total cells L <sup>-1</sup> )
		°N	°N				°N	°W	
6/27/15 8:07	1	28.41	154.45	66.6 (861)	7/20/15 17:14	1	26.25	147.68	82.9 (1,471)
7/10/15 1:06	1	26.69	151.96	91.8 (1,757)	7/31/15 15:31	1	25.80	145.01	95.0 (2,869)
8/17/15 4:01	1	25.10	151.45	78.6 (1,506)	<b>8/02/15 10:09</b>	<b>3</b>	<b>25.24</b>	<b>145.52</b>	<b>42.0 (13,737)</b>
8/18/15 16:37	1	25.15	152.15	15.5 (2,080)	<b>8/03/15 4:29</b>	<b>1</b>	<b>25.00</b>	<b>145.71</b>	<b>29.7 (4,232)</b>
8/19/15 10:55	1	25.18	152.51	78.6 (1,506)	<b>8/03/15 10:38</b>	<b>3</b>	<b>24.93</b>	<b>145.76</b>	<b>56.0 (5,702)</b>
9/2/15 16:29	1	27.44	153.74	64.7 (1,219)	8/05/15 17:34	2	24.71	146.65	85.1 (2,403)
9/27/15 14:14	1	26.12	153.58	100.0 (2,618)	8/08/15 0:22	1	24.81	147.83	80.7 (3,156)
10/15/15 21:22	1	21.80	155.08	95.5 (2,367)	8/08/15 6:31	2	24.81	147.93	100.0 (3,802)
10/20/15 23:22	2	20.81	155.46	69.3 (2,690)	8/09/15 19:10	1	24.86	148.50	39.0 (2,116)
10/21/15 5:28	1	20.77	155.47	31.8 (789)	8/10/15 1:10	1	24.87	148.57	75.8 (2,367)
10/25/15 0:58	2	20.54	155.18	90.1 (2,546)					
10/25/15 7:04	1	20.56	155.11	95.7 (8,249)					
10/25/15 13:10	1	20.54	155.04	100.0 (2,009)					

**Notes:**

The *Hemiaulus* aggregate events outside (left) and within (right) the 15 July–15 August summer export pulse. N = number of aggregates in each 15-image burst at that location. The *Hemiaulus* bloom event is in bold, italicized text.

*Hemiaulus* were present. Aggregates shared common characteristics of curled chains of various sizes tangled together to create a characteristic shape (Fig. 6) and were easily identified when compared to diver-collected aggregates (Fig. S5). When present,  $72 \pm 25\%$  (s.d., n = 23) of the total *Hemiaulus* cells were present in aggregated form (Fig. 8C; Table 2). They were not limited to regions where non-aggregated *Hemiaulus* cells were abundant (Figs. 8C and 8D) and were observed from June 27, 2015 and October 25, 2015 with 13 of the 24 locations outside the time window of the summer export pulse (green shading in Fig. 8D). Within the holograms containing *Hemiaulus* aggregates, the average number of identifiable aggregated cells was  $47 \pm 42$  (s.d., n = 31) with a minimum of seven (two small crossed chains) and a maximum of 220. Due to the complex 3D structures of some of the aggregates, it is likely that cell counts for aggregates are underestimates.

A single aggregate in a 15-image burst represents, on average, 36 aggregates L<sup>-1</sup>. Maximum abundance was present during the *Hemiaulus* bloom (August 2–4, 2015) where normalized abundance was 108 aggregates L<sup>-1</sup>. The highest sustained aggregate abundance was during the early August bloom when aggregates were observed in six of nine successive days (Table 2). However, there was no significant relationship between aggregated and non-aggregated cell abundance ( $r^2 = 0.12$ ,  $p = 0.5$ ,  $n = 23$ ) overall in the data set. On 3 of the 23 bursts where aggregates were observed, they were the only form of *Hemiaulus* present.

The F<sub>v</sub>:F<sub>m</sub> values underwent diel excursions typical of high-light populations experiencing solar-induced photoinhibition and down-regulation of photosynthetic activity where yields were greatest in the dark period and lower during the daytime (Fig. 9A). Crepuscular excursions were evident in many, but not all diel rhythms.

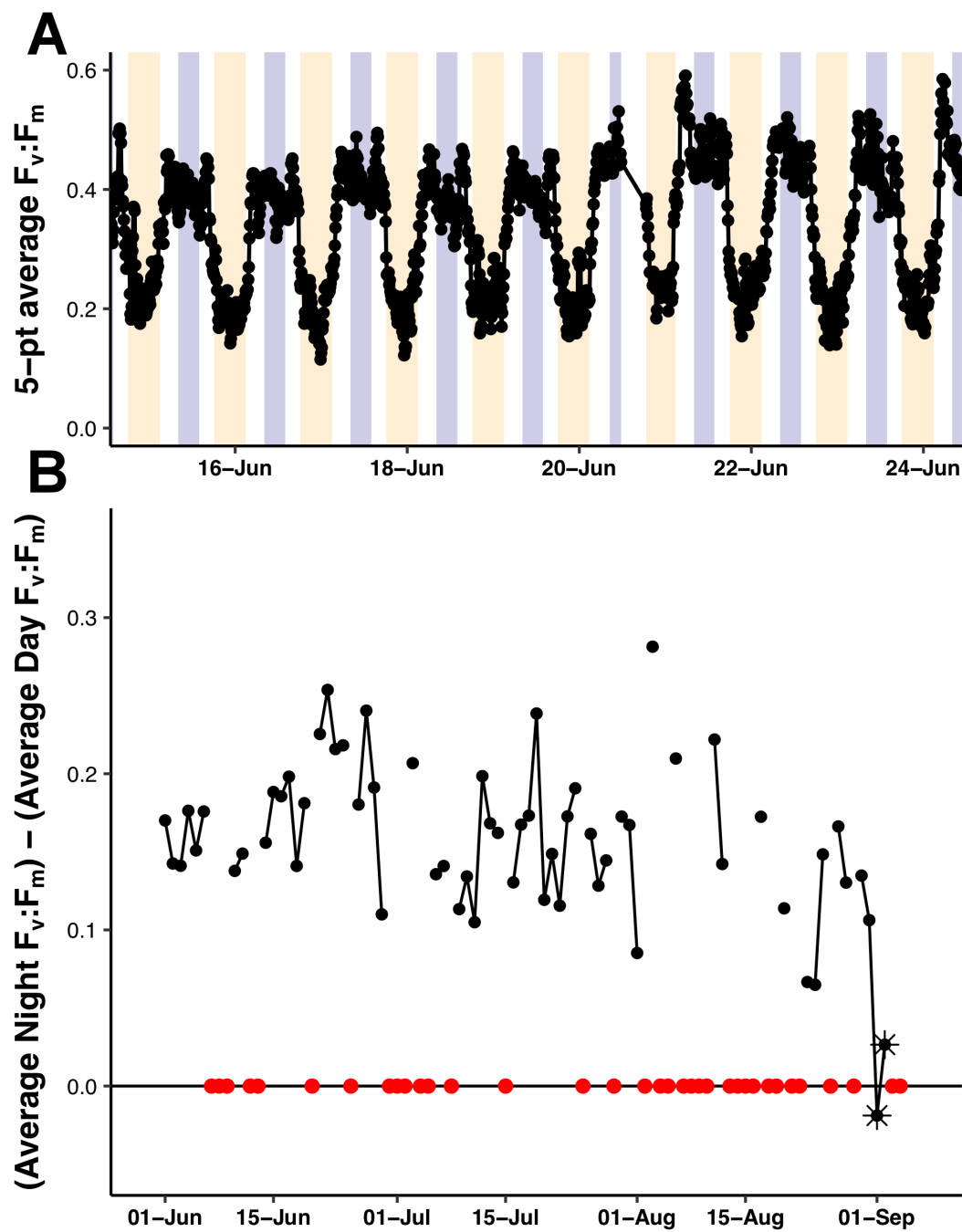


**Figure 9** PhytoFlash  $F_v:F_m$  diel rhythm sample and iron limitation index. (A) Sample of the typical diel rhythm observed in the PhytoFlash  $F_v:F_m$  measurements. The signal is down-regulated during the daytime and returns to the maximum value during the dark period while macro-nutrient limited. Dark bars = 08:00–13:59 UTC (nocturnal period used in the calculation). Light bars = 18:00–02:59 UTC (diurnal period used in the calculation). (B) Time-series of the dark-averaged  $F_v:F_m$  minus the light-averaged  $F_v:F_m$ . Red points indicate where the sample number did not meet the threshold for calculation (see Methods). Asterisks are points where the data was compromised (see Text S1).

Full-size DOI: 10.7717/peerj.5387/fig-9

From visual inspection of the entire mission dataset, there was no reversal of the diel rhythm suggestive of Fe-stress. The quantitative diurnal:nocturnal  $F_v:F_m$  ratio remained positive indicative of a macro-nutrient limited environment (Fig. 9B) although there was a long-term downward slope. The near zero values after September 1, 2015 were the result of compromised PhytoFlash data as the  $F_o$  and  $F_m$  values simultaneously drifted upwards resulting in loss of  $F_v:F_m$  (details in Fig. S6). August 31, 2015 was the last date with uncompromised data before the PhytoFlash completely shutdown on September 9, 2015.

## DISCUSSION

### The Wave Glider SV2 as a sampling platform

The Wave Glider SV2 *Honey Badger* successfully returned from a 5-month mission with all sensors undamaged. All sensors reported data, although at varying frequency and reliability, throughout the mission with the exception of the PhytoFlash. As a prototype mission, it was successful at deploying and recovering optical and imaging sensors specific to phytoplankton research questions. Individual sensors suffered from degradation associated with either platform computer software issues (PhytoFlash) or environmental biofouling (C3s and the LISST-Holo).

Post-mission inspection by Turner Designs indicated the PhytoFlash operated properly when removed from the glider, suggesting the system interface with the glider had failed. The SV2 was the first production model of Wave Gliders. The customized software used to power and communicate with the PhytoFlash was not part of the original system's dedicated software and gradually created insurmountable conflicts that led eventually to a complete failure. The newer generation (SV3) has a more robust on-board computer interface more amenable to customization and this is not likely to be a future issue.

One of the goals of the mission was to sample regions with chl *a* concentrations  $>0.15 \text{ mg m}^{-3}$ . The waypoints for glider were partially chosen based on the Aqua MODIS's chl *a* data. Daily images were often incomplete due to cloud cover as well as being outside the daily imaging path. The 8-day composite of the Aqua MODIS satellite data provided a more complete image of the regional chl *a* concentrations, however, the 8-day images used for daily decision making on the glider's movements were based on data that may have been up to 4-days-old. This delay resulted in a few missed sampling opportunities (Video S1) since chl *a* maps of the region the data were incomplete as waypoints were determined. This was particularly evident in the August *Hemiaulus* bloom. The magnitude of the bloom was not evident in the satellite imagery until the glider was a week past it and nearly halfway to a developing bloom to the west.

### Biological observations

During the June–November timeframe of this mission, *Hemiaulus* and *Rhizosolenia* were the dominant diatom genera observed by the Holo in the NPSG chl *a* blooms, reaffirming *Guillard & Kilham's (1977)* characterization of these taxa as persistent diatom representatives of the oligotrophic open ocean flora. The Holo's resolution limit ( $\sim 15 \mu\text{m}$ ) could not image the smaller pinnate diatoms such as *Mastogloia* that frequently co-dominate in these blooms. The *Hemiaulus* abundance ( $10^4 \text{ cells L}^{-1}$ ) noted in the

August 2–4, 2015 bloom is consistent with previous reports of open Pacific Ocean blooms where *Mastogloia* is a co-dominant (Brzezinski, Villareal & Lipschultz, 1998; Scharek et al., 1999; Venrick, 1974; Villareal et al., 2012). Thus, it is probable that additional diatoms were present and contributing to the satellite chl *a* signature.

The patchiness in the abundance of *Hemiaulus* and the *Rhizosolenia* symbiosis was unexpected. Approximately 2/3 of the bursts contained neither of these taxa. In some cases, the next sampling burst (6 h later, or approximately 10 km) would observe  $\sim 10^3\text{--}10^4$  cells L<sup>-1</sup>. Such variation has been noted before from discrete ship sampling stations (Fong et al., 2008; Venrick, 1974; Villareal et al., 2012) but with little ability to sustain 6 h sampling intervals for months. The most extreme gradients were associated with developing blooms suggesting that the factors driving blooms are highly localized and not represented by the average nutrient or hydrographic characteristics. Calil et al. (2011) reported satellite chl *a* features in this gyre developed rapidly at frontal interfaces between mesoscale features as the result of sub-mesoscale ageostrophic flows resulting in transient up and down welling. This spatial development scale is consistent with the abundance increase noted in the two observed diatom blooms and warrants further investigation into the role that mesoscale frontal features play in diatom-diazotroph association dynamics. However, there are no mechanisms suggested to address the variability in the background concentrations ( $10^1\text{--}10^2$  cell L<sup>-1</sup>) of these taxa presumably adapted to uniformly oligotrophic conditions.

Unlike previous studies using settled water samples or nets, we were able to record and partition *Hemiaulus* into aggregated or unaggregated abundance. *Hemiaulus* aggregates (Villareal et al., 2011) occurred throughout the mission, even in regions of low non-aggregated *Hemiaulus* abundance (Figs. 7 and 9). The presence of one or more aggregates usually dominated the total abundance (Table 2) and on three occasions represented the entire *Hemiaulus* biomass seen. Maximum abundance (108 aggregates L<sup>-1</sup>) and highest sustained aggregate abundance were both present during the *Hemiaulus* bloom (August 2–4, 2015) where aggregated *Hemiaulus* represented 29–56% of the total *Hemiaulus* present in the bursts.

With an aggregate occurrence in 11% of the samples containing *Hemiaulus*, we examine what principles of diatom aggregation are relevant in this environment. Jackson's general coagulation model for diatom aggregates (Jackson, 1990a, 1990b) suggest senescence, elevated concentrations, and enhanced stickiness play a key role in aggregation formation. In our data, aggregate density was highest in the August bloom, consistent with this model. However, the long chains and elevated F<sub>v</sub>:F<sub>m</sub> suggests a rapidly growing *Hemiaulus* population and the continued increase in the bloom area chl *a* after Honey Badger departed (Video S1) suggests that this bloom was sampled early in its development. The aggregated form dominated total abundance when present, and aggregates appeared largely monospecific, at least within the resolution limits of the Holo. In contrast, diatom aggregates in coastal waters scavenge other particles and can sweep the water clear as they sink (Allredge & Gotschalk, 1989, 1990; Allredge & Silver, 1988). We suggest that aggregated forms of *Hemiaulus* are not solely the result of high rates of collision and sticking between *Hemiaulus* cell. Much like *Rhizosolenia*

mats ([Villareal & Carpenter, 1989](#)), they may be a natural growth form of *Hemiaulus* that results from curled chains twisting back on themselves. Further collisions may play a role but appear unlikely in the low density conditions that generally prevailed in this study.

Combined diver and net collections in 2003 ([Villareal et al., 2011](#)) found high *Hemiaulus* abundance was coupled to an aggregation snowstorm ([Fig. S5](#)) and allows us to examine whether the Holo's aggregate abundance data is credible. Using net-collected abundance data from the 2003 bloom (maximum abundance: 2,500 cells L<sup>-3</sup>) and our average cells per aggregates in this study (47 cells), we calculate a potential for ~50 aggregates L<sup>-1</sup> for the 2003 *Hemiaulus* snowstorm. The aggregates visible to divers (centimeter-sized) are substantially larger than the aggregates observed by the Holo (millimeter-sized), so this is likely an overestimate of abundance in the 2003 snowstorm. However, the value is similar to the detection limit represented by one aggregate per 15 image Holo burst (36 aggregates L<sup>-1</sup>) and suggests the Holo data are the correct order of magnitude. Combined with the high proportion of samples containing aggregates (11%), our limited sample volume (~28 mL), the broad aggregate distribution, and the lack of a satellite signature from the 2003 snowstorm ([Villareal et al., 2011](#)), we conclude that dense *Hemiaulus* aggregation events are more common than reported. [Pilskaln et al. \(2005\)](#) reported marine snow aggregates on the order of 1–10 L<sup>-1</sup> at 28–30°N along a transect from HI to CA suggesting that *Hemiaulus* aggregates are part of rich collection of macroscopic particles rarely sampled. The incidental observation from the lookdown camera in a fading bloom of what appeared to be large aggregates in a fading bloom were at too low a density to be sampled by the Holo, but sufficiently large to be visible to the camera ([Fig. S3B](#)). Multiple imaging technologies on the vehicle are clearly needed to further detail this type of event.

Regularly occurring *Hemiaulus* aggregates could be an important food source to organisms in the open ocean due to their high concentration of carbon and nitrogen. They could also play an important role in the global carbon cycle since aggregated forms, when physiologically stressed, tend to sink much faster than non-aggregated particles ([Stemmann & Boss, 2012](#)) and can scavenge other suspended particles as they sink to depth ([Allredge & Silver, 1988](#)). Station ALOHA sediment trap data indicated that during the 13-year record, the summer export pulse resulted in ~20% of the annual carbon export to the benthos at >5,000 m ([Karl et al., 2012](#)) with high sinking rates (10<sup>2</sup> m d<sup>-1</sup>) requiring aggregates as a dominant mode of transport ([Scharek et al., 1999](#); [Scharek, Tupas & Karl, 1999](#)). Our data show that *Hemiaulus* aggregates extend deep into the North Pacific gyre and support the idea that the role of the summer export pulse may be much wider than Station ALOHA waters near Hawai'i. However, there is no evidence that aggregate formation, per se, is linked to the hypothesized annual rhythm driving the summer export pulse. They occur independently of the summer export pulse.

We found no evidence of iron limitation during our sampling with the caveat that the PhytoFlash measures a property of the phytoplankton community present, not a diatom-diazotroph association specific stress. However, even during the *Hemiaulus* and

*Rhizosolenia* blooms observed on August 3, 2015 and August 16, 2015, the Fe index did not suggest iron limitation or iron stress. From June 1, 2015 to August 31, 2015, the dark-averaged  $F_v:F_m$  stayed above the light-averaged values, agreeing with the 2006 study by [Behrenfeld et al. \(2006\)](#) which classified this area as having a type I regime with low macronutrients but sufficient iron supplies.

## CONCLUSIONS

The *Honey Badger* offered a unique look into the remote oligotrophic NPSG during its 5-month, 5,690 km mission. While some of the sensors failed during the mission (PhytoFlash) or produced uninterpretable data (C3s), the mission was a success in that other sensors (LISST-Holo) recorded novel data over an extensive period of time (5 months) and wide geographic extent, and the glider returned intact. The *Honey Badger* and its sensors allowed for a persistent presence in the NPSG during the late summer/early fall bloom season.

The long-term deployment of both imaging and photosynthetic efficiency sensors on a mobile sampling platform provided novel information on the composition and physiology of remote diatom blooms. The region showed no evidence of iron limitation despite the presence of DDAs at  $10^4$  concentrations. *Hemiaulus* aggregates were widespread and observed outside the July 15–August 15 summer export pulse ([Karl et al., 2012](#)) window suggesting that the predictable timing of the summer export pulse cannot be uniquely attributed to a rhythm in aggregate formation. If aggregates are consistent vectors for vertical transport at some stage, then the potential for a basin-wide summer export pulse is enhanced. When present, *Hemiaulus* aggregates are abundant ( $>10 \text{ L}^{-1}$ ) and dominate the total *Hemiaulus* present. Their general characteristics are distinct from coastal diatom aggregates and more similar to *Rhizosolenia* mats ([Allredge & Silver, 1982](#); [Carpenter et al., 1977](#); [Villareal et al., 2014](#)), suggesting *Hemiaulus* aggregates are a natural growth form. Their broad and persistent occurrence suggests they do not have consistently high sinking rates. The PhytoFlash and the Holo data are generally uncoupled from the satellite chl *a* concentrations which illustrates the added value of in situ sampling to understand the community structure and photophysiological characteristics of these blooms in remote open ocean habitats.

## ACKNOWLEDGEMENTS

We wish to thank Liquid Robotics, a Boeing company, for providing the glider time as part of the PacX Challenge award and our project manager Danny Merritt for his contributions to the mission success. We acknowledge John Walpert (GERG) for adapting some of equipment to the SV2. In addition, the skilled field testing and support provided by Brad Woolhiser, Chuck Shaver, Dustin Boettcher, and Vas Podorean at the LR test facility in Kawaihae, HI is gratefully acknowledged. We wish to thank Bob Simons (SWFSC/ERD) for putting the *Honey Badger* data on ERDDAP and Lynn DeWitt (SWFSC/ERD) for creating the project website (<http://oceanview.pfeg.noaa.gov/MAGI>).

## ADDITIONAL INFORMATION AND DECLARATIONS

### Funding

This work was funded by Liquid Robotics, a Boeing company, through a cash grant, glider time, and technical assistance. In addition, this work was supported by the National Science Foundation award OCE 1430048 and 1537546. The funders had no role in study design, data collection and analysis, decision to publish, or preparation of the manuscript.

### Grant Disclosures

The following grant information was disclosed by the authors:

Liquid Robotics.

National Science Foundation award OCE: 1430048 and 1537546.

### Competing Interests

The authors declare that they have no competing interests. Liquid Robotics provided a cash grant, 6 months of Wave Glider time, and technical assistance for this project. They have not seen nor commented on the data or the manuscript.

### Author Contributions

- Emily E. Anderson performed the experiments, analyzed the data, prepared figures and/or tables, authored or reviewed drafts of the paper, approved the final draft.
- Cara Wilson conceived and designed the experiments, performed the experiments, analyzed the data, contributed reagents/materials/analysis tools, prepared figures and/or tables, authored or reviewed drafts of the paper, approved the final draft.
- Anthony H. Knap contributed reagents/materials/analysis tools, authored or reviewed drafts of the paper, approved the final draft, provided expertise in integrating sensors into the vehicle.
- Tracy A. Villareal conceived and designed the experiments, performed the experiments, analyzed the data, contributed reagents/materials/analysis tools, prepared figures and/or tables, authored or reviewed drafts of the paper, approved the final draft.

### Data Availability

The following information was supplied regarding data availability:

Biological and Chemical Oceanography Data Management Office (BCO-DMO): <https://www.bco-dmo.org/project/505589>.

### Supplemental Information

Supplemental information for this article can be found online at <http://dx.doi.org/10.7717/peerj.5387#supplemental-information>.

## REFERENCES

- Agusti S, González-Gordillo JI, Vaqué D, Estrada M, Cerezo MI, Salazar G, Gasol JM, Duarte CM. 2015. Ubiquitous healthy diatoms in the deep sea confirm deep carbon injection by the biological pump. *Nature Communications* 6(1):7608 DOI 10.1038/ncomms8608.

- Alldredge AL, Gotschalk CC.** 1989. Direct observations of the mass flocculation of diatom blooms: characteristics, settling velocities and formation of diatom aggregates. *Deep Sea Research Part A. Oceanographic Research Papers* **36**(2):159–171 DOI [10.1016/0198-0149\(89\)90131-3](https://doi.org/10.1016/0198-0149(89)90131-3).
- Alldredge AL, Gotschalk CC.** 1990. The relative contribution of marine snow of different origins to biological processes in coastal waters. *Continental Shelf Research* **10**(1):41–58 DOI [10.1016/0278-4343\(90\)90034-j](https://doi.org/10.1016/0278-4343(90)90034-j).
- Alldredge AL, Silver MW.** 1982. Abundance and production rates of floating diatom mats (*Rhizosolenia castracanei* and *R. imbricata* var. *shrubsolei*) in the eastern Pacific Ocean. *Marine Biology* **66**(1):83–88 DOI [10.1007/bf00397258](https://doi.org/10.1007/bf00397258).
- Alldredge AL, Silver MW.** 1988. Characteristics, dynamics and significance of marine snow. *Progress in Oceanography* **20**(1):41–82 DOI [10.1016/0079-6611\(88\)90053-5](https://doi.org/10.1016/0079-6611(88)90053-5).
- Behrenfeld MJ, Milligan AJ.** 2013. Photophysiological expressions of iron stress in phytoplankton. *Annual Review of Marine Science* **5**:217–246 DOI [10.1146/annurev-marine-121211-172356](https://doi.org/10.1146/annurev-marine-121211-172356).
- Behrenfeld M, Worthington K, Sherrell RM, Chavez FP, Strutton P, McPhaden M, Shea DM.** 2006. Controls on tropical Pacific Ocean productivity revealed through nutrient stress diagnostics. *Nature* **442**(7106):1025–1028 DOI [10.1038/nature05083](https://doi.org/10.1038/nature05083).
- Bombar D, Moisander PH, Dippner JW, Foster RA, Voss M, Karfeld B, Zehr JP.** 2011. Distribution of diazotrophic microorganisms and nifH gene expression in the Mekong River plume during intermonsoon. *Marine Ecology Progress Series* **424**:39–52 DOI [10.3354/meps08976](https://doi.org/10.3354/meps08976).
- Brzezinski MA, Villareal TA, Lipschultz F.** 1998. Silica production and the contribution of diatoms to new and primary production in the central North Pacific. *Marine Ecology Progress Series* **167**:89–104 DOI [10.3354/meps167089](https://doi.org/10.3354/meps167089).
- Burd AB, Jackson GA.** 2009. Particle Aggregation. *Annual Review of Marine Science* **1**(1):65–90 DOI [10.1146/annurev.marine.010908.163904](https://doi.org/10.1146/annurev.marine.010908.163904).
- Calil PHR, Doney SC, Yumimoto K, Eguchi K, Takemura T.** 2011. Episodic upwelling and dust deposition as bloom triggers in low-nutrient, low-chlorophyll regions. *Journal of Geophysical Research* **116**(C6):C06030 DOI [10.1029/2010jc006704](https://doi.org/10.1029/2010jc006704).
- Calil PHR, Richards KJ.** 2010. Transient upwelling hot spots in the oligotrophic North Pacific. *Journal of Geophysical Research* **115**(C2):C02003 DOI [10.1029/2009jc005360](https://doi.org/10.1029/2009jc005360).
- Capone DG, Zehr JP, Paerl HW, Bergman B, Carpenter EJ.** 1997. Trichodesmium, a globally significant marine cyanobacterium. *Science* **276**(5316):1221–1229 DOI [10.1126/science.276.5316.1221](https://doi.org/10.1126/science.276.5316.1221).
- Carpenter EJ, Capone DG.** 2008. Nitrogen fixation in the marine environment. In: Capone DG, Bronk DA, Mulholland MR, Carpenter EJ, eds. *Nitrogen in the Marine Environment*. San Diego: Elsevier Academic Press Inc, 141–198.
- Carpenter EJ, Harbison RG, Madin LP, Swanberg NR, Biggs DC, Hulbert EM, McAlister VL, McCarthy JJ.** 1977. *Rhizosolenia* mats. *Limnology and Oceanography* **22**:739–741.
- Carpenter EJ, Montoya JP, Burns J, Mulholland MR, Subramaniam A, Capone DG.** 1999. Extensive bloom of a N<sub>2</sub>-fixing diatom/cyanobacterial association in the tropical Atlantic Ocean. *Marine Ecology Progress Series* **185**:273–283 DOI [10.3354/meps185273](https://doi.org/10.3354/meps185273).
- Church MJ, Bjorkman KM, Karl DM, Saito MA, Zehr JP.** 2008. Regional distributions of nitrogen-fixing bacteria in the Pacific Ocean. *Limnology and Oceanography* **53**(1):63–77 DOI [10.4319/lo.2008.53.1.00063](https://doi.org/10.4319/lo.2008.53.1.00063).

- Daniel T, Manley J, Trenaman N.** 2011. The Wave Glider: enabling a new approach to persistent ocean observation and research. *Ocean Dynamics* **61**(10):1509–1520 DOI [10.1007/s10236-011-0408-5](https://doi.org/10.1007/s10236-011-0408-5).
- Davies EJ, Buscombe D, Graham GW, Nimmo-Smith WAM.** 2015. Evaluating unsupervised methods to size and classify suspended particles using digital in-line holography. *Journal of Atmospheric and Oceanic Technology* **32**(6):1241–1256 DOI [10.11175/jtech-d-14-00157.1](https://doi.org/10.11175/jtech-d-14-00157.1).
- Dickey TD, Itsweire EC, Moline MA, Perry MJ.** 2008. Introduction to the Limnology and Oceanography special issue on autonomous and lagrangian platforms and sensors (ALPS). *Limnology and Oceanography* **53**(5part2):2057–2061 DOI [10.4319/lo.2008.53.5\\_part\\_2.2057](https://doi.org/10.4319/lo.2008.53.5_part_2.2057).
- Dore JE, Letelier RM, Church MJ, Lukas R, Karl DM.** 2008. Summer phytoplankton blooms in the oligotrophic North Pacific Subtropical Gyre: historical perspective and recent observations. *Progress in Oceanography* **76**(1):2–38 DOI [10.1016/j.pocean.2007.10.002](https://doi.org/10.1016/j.pocean.2007.10.002).
- Farnelid H, Tarangkoon W, Hansen G, Hansen PJ, Riemann L.** 2010. Putative N<sub>2</sub>-fixing heterotrophic bacteria associated with dinoflagellate–cyanobacteria consortia in the low-nitrogen Indian Ocean. *Aquatic Microbial Ecology* **61**(2):105–117 DOI [10.3354/ame01440](https://doi.org/10.3354/ame01440).
- Fitzpatrick PJ, Lau Y, Moorhead R, Skarke A, Merritt D, Kreider K, Brown C, Canon R, Hine G, Lampoudi T, Leonardi AP.** 2015. A review of the 2014 Gulf of Mexico Wave Glider® field program. *Marine Technology Society Journal* **49**(3):64–71 DOI [10.4031/mtsj.49.3.14](https://doi.org/10.4031/mtsj.49.3.14).
- Follett CL, Dutkiewicz S, Karl DM, Inomura K, Follows MJ.** 2018. Seasonal resource conditions favor a summertime increase in North Pacific diatom–diazotroph associations. *ISME Journal* **12**(6):1543–1557 DOI [10.1038/s41396-017-0012-x](https://doi.org/10.1038/s41396-017-0012-x).
- Fong AA, Karl DM, Lukas R, Letelier RM, Zehr JP, Church MJ.** 2008. Nitrogen fixation in an anticyclonic eddy in the oligotrophic North Pacific Ocean. *ISME Journal* **2**(6):663–676 DOI [10.1038/ismej.2008.22](https://doi.org/10.1038/ismej.2008.22).
- Foster RA, Carpenter EJ, Bergman B.** 2006. Unicellular cyanobionts in open ocean dinoflagellates, radiolarians, and tintinnids: ultrastructural characterization and immuno-localization of phycoerythrin and nitrogenase. *Journal of Phycology* **42**(2):453–463 DOI [10.1111/j.1529-8817.2006.00206.x](https://doi.org/10.1111/j.1529-8817.2006.00206.x).
- Foster RA, O'Mullan GD.** 2008. Nitrogen-fixing and nitrifying symbioses in the marine environment. In: Capone DG, Bronk DA, Mulholland MR, Carpenter EJ, eds. *Nitrogen in the Marine Environment*. Second Edition. San Diego: Elsevier, 1197–1218.
- Foster RA, Zehr JP.** 2006. Characterization of diatom–cyanobacteria symbioses on the basis of nifH, hetR and 16S rRNA sequences. *Environmental Microbiology* **8**(11):1913–1925 DOI [10.1111/j.1462-2920.2006.01068.x](https://doi.org/10.1111/j.1462-2920.2006.01068.x).
- Goebel NL, Edwards CA, Carter BJ, Achilles KM, Zehr JP.** 2008. Growth and carbon content of three different-sized diazotrophic cyanobacteria observed in the subtropical North Pacific. *Journal of Phycology* **44**(5):1212–1220 DOI [10.1111/j.1529-8817.2008.00581.x](https://doi.org/10.1111/j.1529-8817.2008.00581.x).
- Goering JJ, Dugdale RC, Menzel DW.** 1966. Estimates of in situ rates of nitrogen uptake by *Trichodesmium* sp. in the tropical Atlantic Ocean. *Limnology and Oceanography* **11**(4):614–620 DOI [10.4319/lo.1966.11.4.0614](https://doi.org/10.4319/lo.1966.11.4.0614).
- Guidi L, Calil PHR, Duhamel S, Bjoerkman KM, Doney SC, Jackson GA, Li B, Church MJ, Tozzi S, Kolber ZS, Richards KJ, Fong AA, Letelier RM, Gorsky G, Stemmann L, Karl DM.** 2012. Does eddy-eddy interaction control surface phytoplankton distribution and carbon export in the North Pacific Subtropical Gyre? *Journal of Geophysical Research* **117**:G02024 DOI [10.1029/2012jc001984](https://doi.org/10.1029/2012jc001984).
- Guieu C, Aumont O, Paytan A, Bopp L, Law CS, Mahowald N, Achterberg EP, Marañón E, Salihoglu B, Crise A, Wagener T, Herut B, Desboeufs K, Kanakidou M, Olgun N, Peters F,**

**Pulido-Villena E, Tovar-Sanchez A, Völker C.** 2014. The significance of the episodic nature of atmospheric deposition to Low Nutrient Low Chlorophyll regions. *Global Biogeochemical Cycles* **28**(11):1179–1198 DOI [10.1002/2014GB004852](https://doi.org/10.1002/2014GB004852).

**Guillard RRL, Kilham P.** 1977. The ecology of marine planktonic diatoms. In: Werner D, ed. *The Biology of Diatoms*. Berkeley: University of California Press, 346–372.

**Hilton JA, Rachel AF, Tripp HJ, Brandon JC, Jonathan PZ, Villareal TA.** 2013. Genomic deletions disrupt nitrogen metabolism pathways of a cyanobacterial diatom symbiont. *Nature Communications* **4**(1):1767 DOI [10.1038/ncomms2748](https://doi.org/10.1038/ncomms2748).

**Jackson GA.** 1990a. Limitation of algal blooms by formation of flocs through physical coagulation. *EOS* **71**:185.

**Jackson GA.** 1990b. A model of the formation of marine algal flocs by physical coagulation processes. *Deep Sea Research Part A. Oceanographic Research Papers* **37**(8):1197–1211 DOI [10.1016/0198-0149\(90\)90038-w](https://doi.org/10.1016/0198-0149(90)90038-w).

**Jackson GA.** 2005. *Coagulation theory and models of oceanic plankton Aggregation*. Boca Raton: Crc Press-Taylor & Francis Group.

**Karl DM, Church MJ, Dore JE, Letelier RM, Mahaffey C.** 2012. Predictable and efficient carbon sequestration in the North Pacific Ocean supported by symbiotic nitrogen fixation. *Proceedings of the National Academy of Sciences of the United States of America* **109**(6):1842–1849 DOI [10.1073/pnas.1120312109](https://doi.org/10.1073/pnas.1120312109).

**Krause JW, Brzezinski MA, Villareal TA, Wilson C.** 2012. Increased kinetic efficiency for silicic acid uptake as a driver of summer diatom blooms in the North Pacific subtropical gyre. *Limnology and Oceanography* **57**(4):1084–1098 DOI [10.4319/lo.2012.57.4.1084](https://doi.org/10.4319/lo.2012.57.4.1084).

**Kustka A, Carpenter EJ, Sanudo-Wilhelmy SA.** 2002. Iron and marine nitrogen fixation: progress and future directions. *Research in Microbiology* **153**(5):255–262 DOI [10.1016/s0923-2508\(02\)01325-6](https://doi.org/10.1016/s0923-2508(02)01325-6).

**Lee CM, Paluszakiewicz T, Rudnick DL, Omand MM, Todd RE.** 2017. Autonomous instruments significantly expand ocean observing: an introduction to the special issue on autonomous and lagrangian platforms and sensors (ALPS). *Oceanography* **30**(2):15–17 DOI [10.5670/oceanog.2017.211](https://doi.org/10.5670/oceanog.2017.211).

**Lindstrom EJ, NAS A, Shcherbina AY, Rainville L, Farrar JT, Centurioni LR, Dong SF, D'Asaro EA, Eriksen C, Fratantoni DM, Hodges BA, Hormann V, Kessler WS, Lee CM, Riser SC, St Laurent L, Volkov DL.** 2017. Autonomous multi-platform observations during the salinity processes in the upper-ocean regional study. *Oceanography* **30**(2):38–48 DOI [10.5670/oceanog.2017.218](https://doi.org/10.5670/oceanog.2017.218).

**Mills MM, Ridame C, Davey M, La Roche J, Geider RJ.** 2004. Iron and phosphorus co-limit nitrogen fixation in the eastern tropical North Atlantic. *Nature* **429**(6989):292–294 DOI [10.1038/nature02550](https://doi.org/10.1038/nature02550).

**Pilskaln CH, Villareal TA, Dennett M, Darkangelo-Wood C, Meadows G.** 2005. High concentrations of marine snow and diatom algal mats in the North Pacific subtropical gyre: implications for carbon and nitrogen cycles in the oligotrophic ocean. *Deep Sea Research Part I* **52**(12):2315–2332 DOI [10.1016/j.dsr.2005.08.004](https://doi.org/10.1016/j.dsr.2005.08.004).

**Ratten JM, LaRoche J, Desai DK, Shelley RU, Landing WM, Boyle E, Cutter GA, Langlois RJ.** 2015. Sources of iron and phosphate affect the distribution of diazotrophs in the North Atlantic. *Deep Sea Research Part II* **116**:332–341 DOI [10.1016/j.dsr2.2014.11.012](https://doi.org/10.1016/j.dsr2.2014.11.012).

**Scharek R, Latasa M, Karl DM, Bidigare RR.** 1999. Temporal variations in diatom abundance and downward vertical flux in the oligotrophic North Pacific gyre. *Deep Sea Research Part I* **46**(6):1051–1075 DOI [10.1016/s0967-0637\(98\)00102-2](https://doi.org/10.1016/s0967-0637(98)00102-2).

- Scharek R, Tupas LM, Karl DM.** 1999. Diatom fluxes to the deep sea in the oligotrophic North Pacific gyre at Station ALOHA. *Marine Ecology Progress Series* **182**:55–67  
DOI [10.3354/meps182055](https://doi.org/10.3354/meps182055).
- Schreiber U.** 2004. Pulse-Amplitude-Modulation (PAM) fluorometry and saturation pulse method: an overview. In: Papageorgiou GC, Govindjee, eds. *Chlorophyll a Fluorescence. Advances in Photosynthesis and Respiration*. Vol. 19. Dordrecht: Springer, 279–319.
- Stemmann L, Boss E.** 2012. Plankton and particle size and packaging: From determining optical properties to driving the biological pump. *Annual Review of Marine Science* **4**:263–290  
DOI [10.1146/annurev-marine-120710-100853](https://doi.org/10.1146/annurev-marine-120710-100853).
- Subramaniam A, Yager PL, Carpenter EJ, Mahaffey C, Bjorkman K, Cooley S, Kustka AB, Montoya JP, Sanudo-Wilhelmy SA, Shipe R, Capone DG.** 2008. Amazon River enhances diazotrophy and carbon sequestration in the tropical North Atlantic Ocean. *Proceedings of the National Academy of Sciences of the United States of America* **105**(30):10460–10465  
DOI [10.1073/pnas.0710279105](https://doi.org/10.1073/pnas.0710279105).
- Thompson A, Carter BJ, Turk-Kubo K, Malfatti F, Azam F, Zehr JP.** 2014. Genetic diversity of the unicellular nitrogen-fixing cyanobacteria UCYN-A and its prymnesiophyte host. *Environmental Microbiology* **16**(10):3238–3249 DOI [10.1111/1462-2920.12490](https://doi.org/10.1111/1462-2920.12490).
- Thompson AW, Foster RA, Krupke A, Carter BJ, Musat N, Vaulot D, Kuypers MMM, Zehr JP.** 2012. Unicellular cyanobacterium symbiotic with a single-celled eukaryotic alga. *Science* **337**(6101):1546–1550 DOI [10.1126/science.1222700](https://doi.org/10.1126/science.1222700).
- Thomson J, Girton J.** 2017. Sustained measurements of southern ocean air-sea coupling from a wave glider autonomous surface vehicle. *Oceanography* **30**(2):104–109  
DOI [10.5670/oceanog.2017.228](https://doi.org/10.5670/oceanog.2017.228).
- Van Lancker V, Baeye M.** 2015. Wave glider monitoring of sediment transport and dredge plumes in a shallow marine sandbank environment. *PLOS ONE* **10**(6):e0128948  
DOI [10.1371/journal.pone.0128948](https://doi.org/10.1371/journal.pone.0128948).
- Venrick EL.** 1974. The distribution and significance of *Richelia intracellularis* Schmidt in the North Pacific Central Gyre. *Limnology and Oceanography* **19**(3):437–445  
DOI [10.4319/lo.1974.19.3.0437](https://doi.org/10.4319/lo.1974.19.3.0437).
- Venrick EL.** 1988. The vertical distributions of chlorophyll and phytoplankton species in the North Pacific central environment. *Journal of Plankton Research* **10**(5):987–998  
DOI [10.1093/plankt/10.5.987](https://doi.org/10.1093/plankt/10.5.987).
- Venrick EL.** 1999. Phytoplankton species structure in the central North Pacific 1973–1996: variability and persistence. *Journal of Plankton Research* **21**(6):1029–1042  
DOI [10.1093/plankt/21.6.1029](https://doi.org/10.1093/plankt/21.6.1029).
- Villareal TA.** 1992. Marine nitrogen-fixing diatom-cyanobacterial symbioses. In: Carpenter EJ, Capone DG, Reuter J, eds. *Marine Pelagic Cyanobacteria: Trichodesmium and Other Diazotrophs*. Netherlands: Kluwer, 163–175.
- Villareal TA, Adornato L, Wilson C, Shoenbachler CA.** 2011. Summer blooms of diatom-diazotroph assemblages and surface chlorophyll in the North Pacific gyre: a disconnect. *Journal of Geophysical Research* **116**(C3):C03001 DOI [10.1029/2010JC006268](https://doi.org/10.1029/2010JC006268).
- Villareal TA, Brown CG, Brzezinski MA, Krause JW, Wilson C.** 2012. Summer diatom blooms in the North Pacific subtropical gyre: 2008–2009. *PLOS ONE* **7**(4):e33109  
DOI [10.1371/journal.pone.0033109](https://doi.org/10.1371/journal.pone.0033109).
- Villareal TA, Carpenter EJ.** 1989. Nitrogen-fixation, suspension characteristics and chemical composition of *Rhizosolenia* mats in the central North Pacific Gyre. *Biological Oceanography* **6**:327–345.

- Villareal TA, Pilskaln CH, Montoya JP, Dennett M.** 2014. Upward nitrate transport by phytoplankton in oceanic waters: balancing nutrient budgets in oligotrophic seas. *PeerJ* 2:e302 DOI 10.7717/peerj.302.
- Villareal TA, Wilson C.** 2014. A comparison of the Pac-X Trans-Pacific Wave glider data and satellite data (MODIS, Aquarius, TRMM and VIIRS). *PLOS ONE* 9(3):e92280 DOI 10.1371/journal.pone.0092280.
- Weber T, Deutsch C.** 2014. Local versus basin-scale limitation of marine nitrogen fixation. *Proceedings of the National Academy of Sciences of the United States of America* 111(24):8741–8746 DOI 10.1073/pnas.1317193111.
- White AE, Spitz YH, Letelier RM.** 2007. What factors are driving summer phytoplankton blooms in the North Pacific Subtropical Gyre? *Journal of Geophysical Research* 112(C12):C12006 DOI 10.1029/2007jc004129.
- Wilson C.** 2003. Late Summer chlorophyll blooms in the oligotrophic North Pacific Subtropical Gyre. *Geophysical Research Letters* 30(18):1942 DOI 10.1029/2003GL017770.
- Wilson C, Villareal TA, Brzezinski MA, Krause JW, Shcherbina AY.** 2013. Chlorophyll bloom development and the subtropical front in the North Pacific. *Journal of Geophysical Research* 118(3):1473–1488 DOI 10.1002/jgrc.20143.
- Zehr JP, Kudela RM.** 2011. Nitrogen cycle of the open ocean: from genes to ecosystems. *Annual Review of Marine Science* 3:197–225.
- Zehr JP, Waterbury JB, Turner PJ, Montoya JP, Omoregie E, Steward GF, Hansen A, Karl DM.** 2001. Unicellular cyanobacteria fix N<sub>2</sub> in the subtropical North Pacific Ocean. *Nature* 412(6847):635–638 DOI 10.1038/35088063.